A&A 642, A81 (2020)
https://doi.org/10.1051/0004-6361/202038327

Astronomy & Astrophysics

Cool stars in the Galactic center as seen by APOGEE

M giants, AGB stars, and supergiant stars and candidates

M. Schultheis[1], A. Rojas-Arriagada[2,3], K. Cunha[4,5], M. Zoccali[2,3], C. Chiappini[6,7], G. Zasowski[8], A. B. A. Queiroz[6,7], D. Minniti[9,3,10], T. Fritz[11,12], D. A. García-Hernández[11,12], C. Nitschelm[13], O. Zamora[11,12], S. Hasselquist[8,⋆], J. G. Fernández-Trincado[14], and R. R. Munoz[15]

[1] Université Côte d'Azur, Observatoire de la Côte d'Azur, Laboratoire Lagrange, CNRS, Blvd de l'Observatoire, 06304 Nice, France
e-mail: mathias.schultheis@oca.eu
[2] Instituto de Astrofísica, Facultad de Física, Pontificia, Universidad Católica de Chile, Av. Vicuña Mackenna 4860, Santiago, Chile
[3] Millennium Institute of Astrophysics, Av. Vicuña Mackenna 4860, 782-0436 Macul, Santiago, Chile
[4] University of Arizona, Tucson, AZ 85719, USA
[5] Observatório Nacional, Sao Cristóvao, Rio de Janeiro, Brazil
[6] Leibniz-Institut für Astrophysik Potsdam (AIP), An der Sternwarte 16, 14482 Potsdam, Germany
[7] Laboratório Interinstitucional de e-Astronomia, – LIneA, Rua Gal. Joseé Cristino 77, Rio de Janeiro, RJ 20921-400, Brazil
[8] Department of Physics & Astronomy, University of Utah, Salt Lake City, UT 84112, USA
[9] Departamento de Ciencias Fisicas, Facultad de Ciencias Exactas, Universidad Andres Bello, Av. Fernandez Concha 700, Las Condes, Santiago, Chile
[10] Vatican Observatory, V00120 Vatican City State, Italy
[11] Instituto de Astrofísica de Canarias, Calle Via Láctea s/n, 38206 La Laguna, Tenerife, Spain
[12] Universidad de La Laguna (ULL), Departamento de Astrofísica, 30206 La Laguna, Tenerife, Spain
[13] Centro de Astronomía (CITEVA), Universidad de Antofagasta, Avenida Angamos 601, Antofagasta 1270300, Chile
[14] Instituto de Astronomía y Ciencias Planterias, Universidad de Atacama, Copayapu 485, Copiapó, Chile
[15] Departamento de Astronomia, Universidad de Chile, Camino El Observatorio 1515, Las Condes, Santiago, Chile

Received 3 May 2020 / Accepted 22 August 2020

ABSTRACT

The Galactic center region, including the nuclear disk, has until recently been largely avoided in chemical census studies because of extreme extinction and stellar crowding. Large, near-IR spectroscopic surveys, such as the Apache Point Observatory Galactic Evolution Experiment (APOGEE), allow the measurement of metallicities in the inner region of our Galaxy. Making use of the latest APOGEE data release (DR16), we are able for the first time to study cool Asymptotic Giant branch (AGB) stars and supergiants in this region. The stellar parameters of five known AGB stars and one supergiant star (VR 5-7) show that their location is well above the tip of the red giant branch. We studied metallicities of 157 M giants situated within 150 pc of the Galactic center from observations obtained by the APOGEE survey with reliable stellar parameters from the APOGEE pipeline making use of the cool star grid down to 3200 K. Distances, interstellar extinction values, and radial velocities were checked to confirm that these stars are indeed situated in the Galactic center region. We detect a clear bimodal structure in the metallicity distribution function, with a dominant metal-rich peak of [Fe/H] $\sim$ +0.3 dex and a metal-poor peak around [Fe/H] = −0.5 dex, which is 0.2 dex poorer than Baade's Window. The α-elements Mg, Si, Ca, and O show a similar trend to the Galactic bulge. The metal-poor component is enhanced in the α-elements, suggesting that this population could be associated with the classical bulge and a fast formation scenario. We find a clear signature of a rotating nuclear stellar disk and a significant fraction of high-velocity stars with $v_{\rm gal} > 300\,{\rm km\,s^{-1}}$; the metal-rich stars show a much higher rotation velocity ($\sim$200 km s^{-1}) with respect to the metal-poor stars ($\sim$140 km s^{-1}). The chemical abundances as well as the metallicity distribution function suggest that the nuclear stellar disk and the nuclear star cluster show distinct chemical signatures and might be formed differently.

Key words. Galaxy: bulge – Galaxy: stellar content – stars: fundamental parameters – stars: abundances

1. Introduction

The Milky Way bulge is such a complex system that its formation and evolution are still poorly understood. As a result of high extinction and crowding, the study of the Galactic bulge remains challenging. Extinction of more than 30 mag in A_V in the Galactic center (GC) regions requires IR spectroscopy. While an increasing number of detailed chemical abundances in the intermediate and outer bulge (such as Baade's Window) are now available thanks to large spectroscopic surveys such as ARGOS (Freeman et al. 2013), *Gaia*-ESO (Rojas-Arriagada et al. 2014), and APOGEE (García Pérez et al. 2013), chemical abundances of stars in the inner Galactic bulge (IGB) with projected distances of $R_G \leq 200$ pc from the GC remain poorly studied.

There have been a few earlier works dedicated to studying the chemistry of stars in the central part of the Milky Way. Using high-resolution IR spectra ($R \sim 40\,000$), Carr et al. (2000) made the first detailed abundance measurement of a star in the GC within 1 pc, the M2 supergiant IRS 7, finding roughly solar metallicity and an abundance pattern that was consistent with the dredge-up of CNO cycle products. Ramírez et al. (2000) also analyzed high-resolution IR spectra ($R = 40\,000$) of a

⋆ NSF Astronomy and Astrophysics Postdoctoral Fellow.

sample of ten cool supergiant and red-giant stars in the GC and estimated an iron abundance of $+0.12 \pm 0.22$ dex. Subsequently, Cunha et al. (2007) used $R \sim 50\,000$ spectra to study the detailed chemistry of the Ramírez et al. (2000) sample and found a slightly enhanced and narrow metallicity distribution ($\langle$[Fe/H]$\rangle = +0.14 \pm 0.06$ dex) that was also alpha enhanced; we note that this small sample of 10 stars, save for one, were members of the central cluster. More recently, Ryde & Schultheis (2015, RS2015) studied nine field stars with projected distances of $R \leq 50$ pc and also found a metal-rich population with [Fe/H] $= +0.11 \pm 0.15$ dex and a lack of a metal-poor population (similarly to Cunha et al. 2007), but found low [α/Fe] values, except for calcium. Their mean metallicities are ∼0.3 dex higher than fields in the inner bulge (Rich et al. 2007, 2012), indicating that the GC region contains a distinct population. A refined analysis (Nandakumar et al. 2018) gave a slightly higher mean metallicity of [Fe/H] $= +0.3 \pm 0.10$ dex and confirmed the very narrow distribution. Grieco et al. (2015) compared these data with a chemical evolution model and concluded that in order to reproduce the observed [α/Fe] ratios, the GC region should have experienced a main strong burst of star formation and should have evolved very quickly with an IMF containing more massive stars.

More recently, Schultheis et al. (2019) found evidence of a chemically distinct population in the nucleus (nuclear stellar disk (NSD) and nuclear star cluster (NSC)) compared to the IGB that shows a very high fraction of metal-rich stars (∼80%) with a mean metallicity of +0.2 dex in the GC. They concluded that the nucleus mimics a metallicity gradient of ~ -0.27 dex kpc^{-1} in the inner 600 pc but is flat if the GC is excluded.

Schultheis et al. (2015) (hereafter referred to as S15) studied 33 M giant stars of APOGEE in the so-called GALCEN field to study the metallicity distribution function and chemical abundances using the DR12 data release (Alam et al. 2015). However, they had to limit their analysis to stars with $T_{\rm eff} > 3700$ K, due to problems modeling the coolest stars (Holtzman et al. 2015), thus excluding a large number of cool stars (including asymptotic giant branch stars (AGB) and supergiants) from their analysis. They found some evidence of the presence of a metal-poor fraction of stars that are α-enhanced.

In this paper, we take advantage of the recently released and improved results from APOGEE DR16 (Ahumada et al. 2020), which has several improvements over previous data releases, in particular DR12 (see details in Jönsson et al. 2020), and includes additional observations of one plate at APOGEE-S that is dedicated to observations of targets in the GC. It is most relevant to the study of cool luminous stars in the central parts of the Milky Way that the DR16 results now cover effective temperatures as low as 3200 K using the grid of spherical MARCS model atmospheres (Gustafsson et al. 2008). In this paper, we present results for the metallicity distribution function and chemical abundances of 157 M giants, which constitutes one of the largest high-resolution spectroscopic samples in the inner degree of the Milky Way to date. In addition, this is the first study of cool AGB stars and supergiants in the GALCEN field using results from the APOGEE survey.

2. The sample

2.1. APOGEE

The Apache Point Observatory Galactic Evolution Experiment (APOGEE) is a large scale, near-IR high-resolution ($R \sim 22\,500$) spectroscopic survey of the Milky Way stellar populations, which is mainly focused on red giants (Majewski et al. 2017; Zasowski et al. 2013, 2017). APOGEE has been a component of both SDSS-III and SDSS-IV (Eisenstein et al. 2011; Blanton et al. 2017) and uses custom-built twin spectrographs at the Apache Point Observatory's 2.5 m Sloan Telescope and Las Campanas Observatory's 2.5 m du Pont telescope (Gunn et al. 2006; Wilson et al. 2019). APOGEE observes in the H-band, where extinction by dust is significantly lower than at optical wavelengths (e.g., $A(H)/A(V) \sim 0.16$).

With its high resolution and high S/N (∼100 per Nyquist-sampled pixel), APOGEE determines both accurate radial velocities (better than 0.5 km s^{-1}) and reliable abundance measurements, including the most abundant metals in the universe (C, N, O), along with other α, odd-Z, and iron-peak elements. The latest SDSS-IV data release (DR16; Ahumada et al. 2020) provides the scientific community with spectra of more than 430 000 stars, as well as the derived stellar properties, including radial velocities, effective temperatures, surface gravities, metallicities, and individual abundances. Additional information, such as photometry and target selection criteria, is also provided and described in Zasowski et al. (2013, 2017). Stellar parameters and chemical abundances for up to 24 elements were derived by the APOGEE Stellar Parameters and Chemical Abundances Pipeline (ASPCAP, García Pérez et al. 2016), while in Nidever et al. (2015) the data reduction and radial velocity pipelines are described. The model grids are based on a complete set of MARCS stellar atmospheres (Gustafsson et al. 2008), and the spectral synthesis using the Turbospectrum code (Alvarez & Plez 1998,Plez 2012) with a new updated line list has been used (Smith et al., in prep.).

In addition to DR16, we use additional observations including additional stars observed after those released in DR16 from APOGEE-S. These data were reduced with the same pipeline as the DR16 stars.

2.2. Distances

We obtained the StarHorse (SH) distances from Queiroz et al. (2020a) for the latest APOGEE-2 survey data release DR16, as well as for the additional stars not present in DR16. The SH is a Bayesian fitting code that derives distances and extinction as well as other quantities such as ages and masses. For more details about the method, the priors, and its validation, we refer the reader to Queiroz et al. (2018, 2020a) which combines the ASPCAP stellar parameters with *Gaia* DR2 and photometric surveys thus achieving precise distances and extinction; the extinction treatment has been significantly improved in the updated version. The typical internal precision in distance for our GALCEN DR16 sample is about 10 ± 7%. The SH uses the APOGEE targeting extinction estimate (see Zasowski et al. 2013, 2017) as a prior for the total line-of-sight extinction. In addition, we also did a comparison with the 3D extinction map of Schultheis et al. (2014) using VVV data and the 2D extinction map of Gonzalez et al. (2012), where we find similar A_K values (within 10% uncertainty) with respect to RJCE.

2.3. The GALCEN field

Two plates of GALCEN, one at APO (location ID 4330) and one at LCO (location ID 5534), have been observed with a total number of 619 stars. Due to the high interstellar extinction, a special target selection procedure was applied for the GALCEN field

(Zasowski et al. 2013). Known AGB long-period variables based on K-band light curves (Matsunaga et al. 2009) were targeted, as well as spectroscopically identified supergiants such as IRS7, IRS19, and IRS22, and supergiant candidates based on photometric color-color criteria. These AGB and supergiant targets have among the coolest effective temperatures ($T_{\rm eff}$ < 3500 K) in the APOGEE stellar sample. While in S15 due to the limiting ATLAS9 model atmospheres grid in ASPCAP for cool stars, only 33 warm K/M giants were used, for this paper we made use of the cooler model grid of MARCS model atmospheres to quadruple the sample.

One of the most significant improvements of DR16 compared to DR14 is the accuracy and consistency of the derived stellar parameters for the coolest giants ($T_{\rm eff}$ < 3500 K), which is due to the use of MARCS model atmospheres in spherical symmetry. This improvement can be clearly seen by the visual inspection of the HR diagram (see e.g., Fig. 3), and notably the "clumpiness" of the HR diagram with $T_{\rm eff}$ < 3500 K seen in DR14 is now gone (see Jönsson et al. 2020). However, "external" calibrators for these cool stars are lacking, which would be important for estimating the accuracy of the stellar parameters for those objects.

For our selection, we disregarded stars with ASPCAPFLAGS=='STAR'BAD" and STARFLAGS = "PERSISTHIGH", as well as telluric standard stars, leaving us with a total number of 270 stars. Those 270 include five known AGB stars and one supergiant star (VR 5-7) in our sample. Table A.1 shows the stellar parameters for those stars.

From the 270 stars, AGB/supergiant candidates have been chosen as those brighter than H < 12.2, 1.3 < $H - K$ < 3.7, which excludes AGB/supergiant stars with strong IR excess, and $K_0 = K - (1.82 * ((H - K) - 0.2))$ < 4.7, which is the dereddened magnitude to put the star above the AGB tip. We note that the more massive (>3–4 solar masses) and O-rich AGB stars can be brighter (because of flux contribution by hot bottom burning) than the AGB theoretical luminosity limit (see e.g., García-Hernández et al. 2009), and that to unambiguously distinguish between AGB or supergiant status, one would need to have photometric light curves and/or some key chemical information from optical spectra (e.g., lithium and s-process elements; García-Hernández et al. 2006, 2007, see also García-Hernández 2017 for a review). The factor 1.82 corresponds to the $A_K/E(H-K)$ ratio from Indebetouw et al. (2005). The 15 AGB/supergiant candidate stars in our final sample, together with their stellar parameters, are given in Table 2.

Figure 1 shows the dereddened color-magnitude diagram of the full GALCEN sample, together with the known AGB/supergiant stars and candidate AGB/supergiant stars, colored by the galactocentric radius. As AGB stars and supergiants have circumstellar material due to their mass-loss, the dereddenings of those stars were obtained by obtaining the median $E(J-K)$ color excess from the VVV extinction map (Gonzalez et al. 2012) instead of the APOGEE estimate. Clearly visible is the foreground contribution with $(J-K)_0$ < 0.8, which can easily be removed by a simple distance cut. The AGBs and supergiants (both known and candidates) are the most luminous stars and they lie well above the tip of the red giant branch (RGB) with K_0 = 7.9 (Habing & Olofsson 2004), as indicated by the dashed line. By imposing a cut-off in $R_{\rm GC}$ < 3.5 kpc, a total of 157 stars are left over for our analysis. We refer to this later on as the GALCEN sample.

Figure 2 shows the spatial distribution of the GALCEN sample in Galactic coordinates superimposed on the interstellar extinction map of Gonzalez et al. (2012). In the highest extincted

Table 1. Known AGB and supergiants with stellar parameters from APOGEE-DR16.

2MASS ID	$T_{\rm eff}$	log g	[M/H]	Ref.
2M17451937-2914052	3730	0.34	−0.28	A58 (1)
2M17445261-2914110	3244	0.12	0.13	A20 (1)
2M17452187-2913443	3290	0.38	0.21	A62 (1)
2M17460808-2848491	3555	0.43	−0.46	V5009Sgr (2)
2M17461658-2849498	3242	0.12	−0.15	VR 5-7 (3,4)

References. (1) Schultheis et al. (2003), (2) Matsunaga et al. (2009), (3) Davies et al. (2009), (4) Cunha et al. (2007).

Table 2. Supergiant candidates.

2MASS ID	$T_{\rm eff}$	log g	[M/H]
2M17460746-2846416	3584	0.95	0.29
2M17461382-2825206	3741	0.86	−0.24
2M17461772-2841159	3221	−0.02	−0.12
2M17462661-2819422	3218	−0.38	−0.26
2M17463072-2850325	3327	0.31	0.13
2M17463266-2837184	3692	0.55	−0.11
2M17463693-2820212	3346	0.90	0.13
2M17463769-2841257	3129	−0.15	−0.08
2M17464409-2817487	3128	−0.14	−0.05
2M17464864-2818274	3181	0.35	0.40
2M17471240-2838377	3536	0.31	−0.59
2M17472459-2822320	3337	0.03	−0.09
2M17472709-2840356	3360	0.23	−0.05
2M17480017-2821058	3292	0.23	0.13

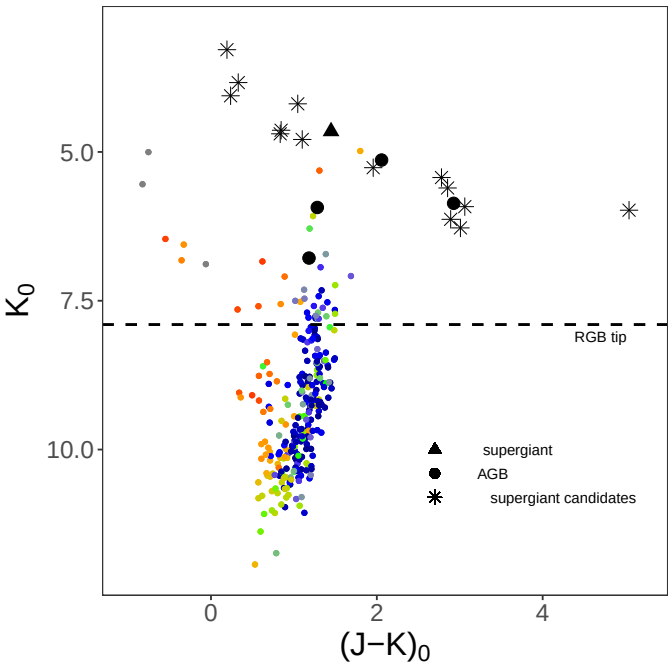

Fig. 1. Dereddened color-magnitude diagram of the GALCEN sample as a function of the galactocentric distance. Superimposed are known AGB stars (filled circles), known supergiants (filled triangles) and AGB/supergiant candidates (asterisks) based on photometric selection criteria (see text).

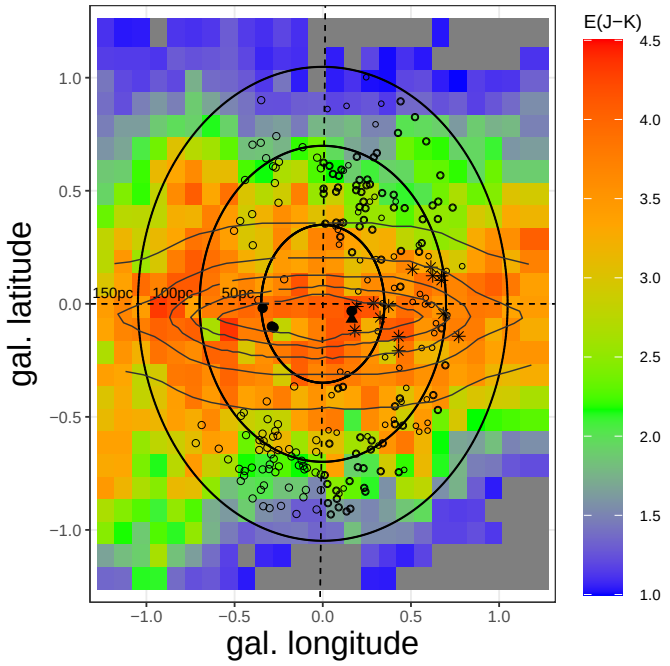

Fig. 2. Galactic-longitude vs. Galactic-latitude distribution of the GALCEN sample superimposed on the interstellar extinction map of Gonzalez et al. (2012). The circles denote radii of 50 pc, 100 pc, and 150 pc assuming a distance to the GC of 8.2 kpc. Open circles denote M giant stars, the filled triangle is the supergiant VR 5-7, filled circles are AGB stars (see Table 1), and asterisks are supergiant candidates (see Table 2). The gray contours show the surface brightness map of the best fit model of the nuclear bulge component by Launhardt et al. (2002).

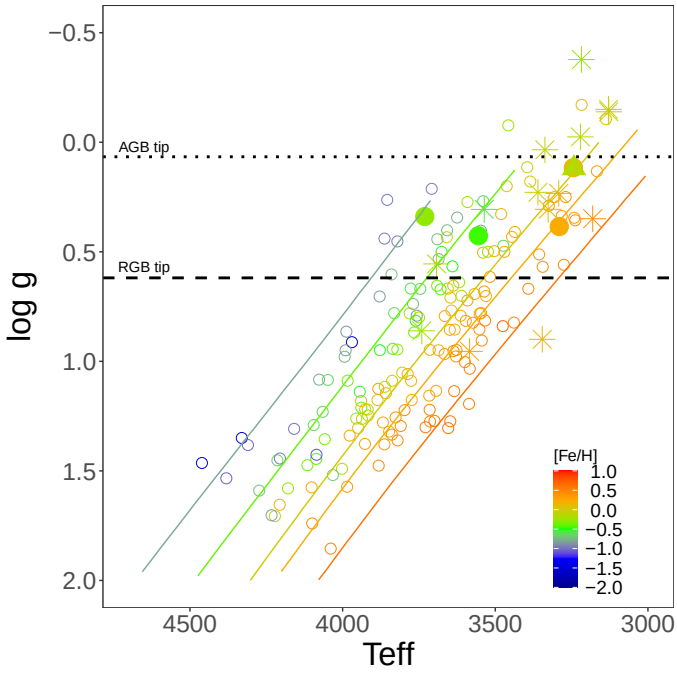

Fig. 3. Teff vs. $\log g$ as function of metallicity together with PARSEC isochrones with an age of 8 Gyr. Indicated are AGB stars as filled circles, supergiants as filled triangles, and supergiant candidates as asterisks. The dotted line shows the approximate location of the tip of the AGB, while the dashed line shows the tip of the RGB (see text).

regions, mainly AGB stars (filled circles), supergiants (filled triangle), and supergiant candidates (asterisks) are located with projected distances closer than 50 pc to SgrA*. The majority of the M giants in our sample are located in relatively low extinction windows with $E(J-K) < 3.0$ with projected distances of 50–150 pc away from the GC. We also superimposed the stellar mass distribution of the nuclear disk from Launhardt et al. (2002).

Stellar parameters and chemical abundances of up to 24 elements are determined by the ASPCAP pipeline (see García Pérez et al. 2016). These values are based on a χ^2 minimization between observed and synthetic model spectra (see Zamora et al. 2015 and Holtzman et al. 2015 for more details on the DR16 spectral libraries) performed with the FERRE code (Allende Prieto et al. 2006, and subsequent updates).

Figure 3 shows the HR diagram of the GALCEN sample colored by the metallicity. Superimposed are PARSEC isochrones (Pastorelli et al. 2019) assuming an age of 8 Gyr. Indicated are the approximate limits of the RGB with $M_{\rm bol} < -3.5$ (Habing & Olofsson 2004) and the tip of the AGB with $M_{\rm bol} = -7.0$ (Schultheis et al. 2003). However, as pointed out by McQuinn et al. (2019), the tip of the RGB becomes brighter for metal-rich stars with up to 0.3 mag difference in the K-band (see their Fig. 6). The spread in the effective temperature at a given surface gravity is mainly due to the metallicity, nicely also indicated by the isochrones. The known AGB stars are situated above the tip of the RGB and show similar metallicities as would be expected from their location in the HR diagram following the stellar isochrones. We notice, however, two stars (2M17462584-2850001 and 2M17470135-2831410) that show very low metallicities ([Fe/H] < -2.0) where their projected metallicities on the HR diagram do not match the isochrone metallicities. Their ASPCAP fits are particularly bad (i.e., relatively high χ^2 values). One of these stars (2M17462584-2850001) is a known AGB star with a Mira-like long variability period of 519 days, while the other star (2M17470135-2831410) is an AGB/supergiant candidate with no period information available but with a near-IR variability more typical of an extreme AGB star. The automatic pipeline ASPCAP does not work well for extreme AGB/supergiant stars (e.g., the more massive and/or evolved dusty AGBs or extreme and dusty red supergiants; APOGEE/ASPCAP team, priv. comm.). For the very few known extreme Galactic disk (solar metallicity), O-rich AGB stars observed by APOGEE, ASPCAP systematically gives much lower metallicities (even by 2 dex) for the longer period stars, which are expected to be the more massive and/or evolved dusty AGBs. There are several reasons for this, such as veiling by hot dust emission, stronger degeneracies due to their much more complex spectra, and/or the specific pulsational phase during the observations, with the first one very likely being the dominant factor. This is because the strong hot dust emission in these stars veils the spectrum and the molecular bands look much weaker than reality; ASPCAP could thus compensate this with a much lower global metallicity and/or a higher Teff. Thus, we are not confident about the ASPCAP results for these two particular and extreme stars.

3. AGB stars and supergiants

3.1. Previously known AGB stars and supergiants

Schultheis et al. (2003) (hereafter referred to as S03) performed low-resolution spectroscopic follow-up observations of sources with bright excess 7 and 15μm from the ISOGAL survey

(Omont et al. 2003), which probed the stellar populations of the inner region of the Milky Way. The majority of these sources are long-period variables on the AGB with strong mass-loss, and they are well traced by their 15 μm excess (Glass et al. 1999). Indeed, S03 showed that the molecular bands of ^{12}CO and H_2O, together with the bolometric magnitudes, are an excellent indicator of stellar populations such as AGB stars, supergiants, red giants and young stellar objects.

2M17451937-2914052 is a high-luminosity OH/IR star from the OH/IR star sample of Ortiz et al. (2002). These are the most extreme AGB stars, with large pulsational periods (several hundreds of days) and mass-loss rates up to a few times $10^{-5}\,M_{\odot}\,\mathrm{yr}^{-1}$, displaying the highest bolometric luminosities ($M_{\rm bol} < -4$). Furthermore, S03 estimated the $M_{\rm bol} \sim -5.13$ and the mass-loss rate of $8 \times 10^{-6}\,M_{\odot}\,\mathrm{yr}^{-1}$. The Near-IR, low-resolution spectrum of S03 shows extremely strong water absorption at about 1.7 μm, typical for large amplitude pulsation (see e.g. Lançon & Wood 2000).

2M17462584-2850001 is also a known OH/IR star that was monitored by Wood et al. (1998) and also appears in the catalog of large amplitude variables of Glass et al. (2001) and Matsunaga et al. (2009). It has a period of 505 days (compared to 519 days in Matsunaga et al. 2009) and an amplitude in K of 1.60 mag. It has a very low ASPCAP metallicity of [Fe/H] $\sim$ −2.17 compared to the others. The ASPCAP χ^2 value is higher than 100, compared to a typical value of about 20–50 for the other stars, making the stellar parameters, including the global metallicity, unreliable. We omit this star from our study.

2M17445261-2914110 and 2M17452187-2913443 are classified by S03 as AGB star candidates with $M_{\rm bol} = -4$ and −4.77, respectively. They have moderate mass-loss rates of $\sim 7.4 \times 10^{-7}$ and $2 \times 10^{-7}\,M_{\odot}\,\mathrm{yr}^{-1}$, respectively. They both also show some moderate water absorption. 2M17460808-2848491 is a large-amplitude Mira Variable, first discovered by Glass et al. (2001) and reconfirmed by Matsunaga et al. (2009). It has a period of 297 days with an K amplitude of 0.55 mag.

2M17461658-2849498 (VR 5-7) is a member of the Quintuplet Cluster (Moneti et al. 1994) and has been classified as a supergiant with a spectral type of M6I (Liermann et al. 2009). Cunha et al. (2007) obtained a photometric temperature (based on the measurements of the CO molecular band) of 3600 K, a photometric $\log g$ of −0.15 dex, and an iron abundance of +0.14 dex. Davies et al. (2009) observed VR 5-7 in the H-band at Keck with NIRSPEC and a spectral resolution of 17 000. They obtained a $T_{\rm eff}$ of 3400 ± 200 K, a $\log g$ of 0.0 ± 0.3 dex, and a [Fe/H] = 0.10 ± 0.11 dex. While the temperature and surface gravity agrees within the errors, the metallicity of APOGEE is about 0.2 dex lower.

Figure 4 shows the APOGEE spectrum of VR 5-7 together with the best fit model of ASPCAP (in red). We clearly see the strong impact of the molecular lines such as CN, OH, and CO (indicated in gray, orange, and lime, respectively).

3.2. AGB/supergiant candidates

As mentioned in Sect. 2.3, AGB/supergiant candidates were chosen using a photometric color-cut in H–K, as well as the dereddened magnitude cut of K_0 to put the star above the tip of the AGB. In total, 15 AGB/supergiant candidates are in our sample with the stellar parameters given in Table 2. Twelve stars out of fifteen indeed lie above the tip of the RGB in Fig. 3, and five of them are even above the tip of the AGB. One of them, 2M17463266-2837184, shows an extreme $(J-K)_0$ color of about 5 and could be an AGB star with strong mass loss. The three remaining stars are only about 0.2–0.3 dex below the tip of the RGB, which is approximately the uncertainties of the derived surface gravities of APOGEE for those kinds of objects. This shows that a photometric H–K cut together with the dereddened K magnitude is a priori a good first indication of detecting M AGB/supergiants. Three additional stars lie above the tip of the AGB and also show very high luminosities in the CMD (Fig. 1), making them excellent candidates for being supergiant stars. The relatively high fraction of supergiants in GALCEN is compatible with a recently increased star formation rate during the last 200–300 Myr (Pfuhl et al. 2011).

4. Metallicity distribution function

Schultheis et al. (2015) already had some indications for the existence of a metal-poor population in the GC region based on their metallicity distribution function (MDF) as shown in their Fig. 4. With our larger sample here, we performed a Gaussian mixture modeling (GMM) decomposition, which is a parametric probability density function given by the weighted sum of a number of Gaussian components. In order to constrain the number of Gaussians, we adopted the Akaike information criterion (AIC), which favours a two-component solution. For comparison, we also performed a GMM for BW with the same sample criteria, defined as in Schultheis et al. (2017) but applied to the DR16 data release.

In both samples (GALCEN and BW), we find a narrow metal-rich component and a broader metal-poor component. The metal-rich component of both fields are centered at around [Fe/H] = +0.3 dex, with a slightly larger dispersion for the GALCEN field. Very striking and visible is the metal-poor peak in the GALCEN field centered at [Fe/H] = −0.53 dex. This is about 0.2 dex more metal-poor than the equivalent peak in BW, while the dispersions are very similar (∼0.4 dex). Sixty-three percent of the population in BW is in the metal-poor regime, while for the GALCEN field it is about 47% (73 stars out of 157).

In order to test the statistical significance, we performed a bootstrapping analysis with 1000 resamplings. For BW, we find the metal-rich peak at [Fe/H] = −0.33 ± 0.03, and [Fe/H] = 0.38 ± 0.01 for the metal-poor component, while for GALCEN the two components are situated at [Fe/H] = 0.30 ± 0.03 and [Fe/H] = −0.54 ± 0.08, respectively. The mean weight of the metal-poor component of BW is 62.8 ± 3.6% while for GALCEN it is 46.6 ± 6.3% leading to a statistically significant difference of 2.23 sigma.

Indicated in green are also the four previously known AGB stars and the supergiant star VR 5-7, as well as the AGB/supergiant candidates. A visual inspection of the overall shape of the MDF of these cool stars shows that they follow the general trend of the normal red giants. This gives us confidence that the metallicities of those cool stars are indeed reliable. Unfortunately, the sample size is too small to perform any statistical tests. We also notice that the dispersion in the metallicity for these stars is much narrower (∼0.25 dex) compared to the M giants, however its is clear that a larger sample size is needed in order to attribute differences in the MDF.

Zoccali et al. (2017) used simple limits of [Fe/H] > +0.1 to define metal-rich stars and [Fe/H] < −0.1 for the metal-poor ones to argue that the metal-rich population of their GIBS data is flattened and concentrated toward the Galactic plane, while the metal-poor component is spheroidal. Schultheis et al. (2019) used these same criteria to detect a very prominent metallicity spike (see their Fig. 4) in the GC (including the nuclear star

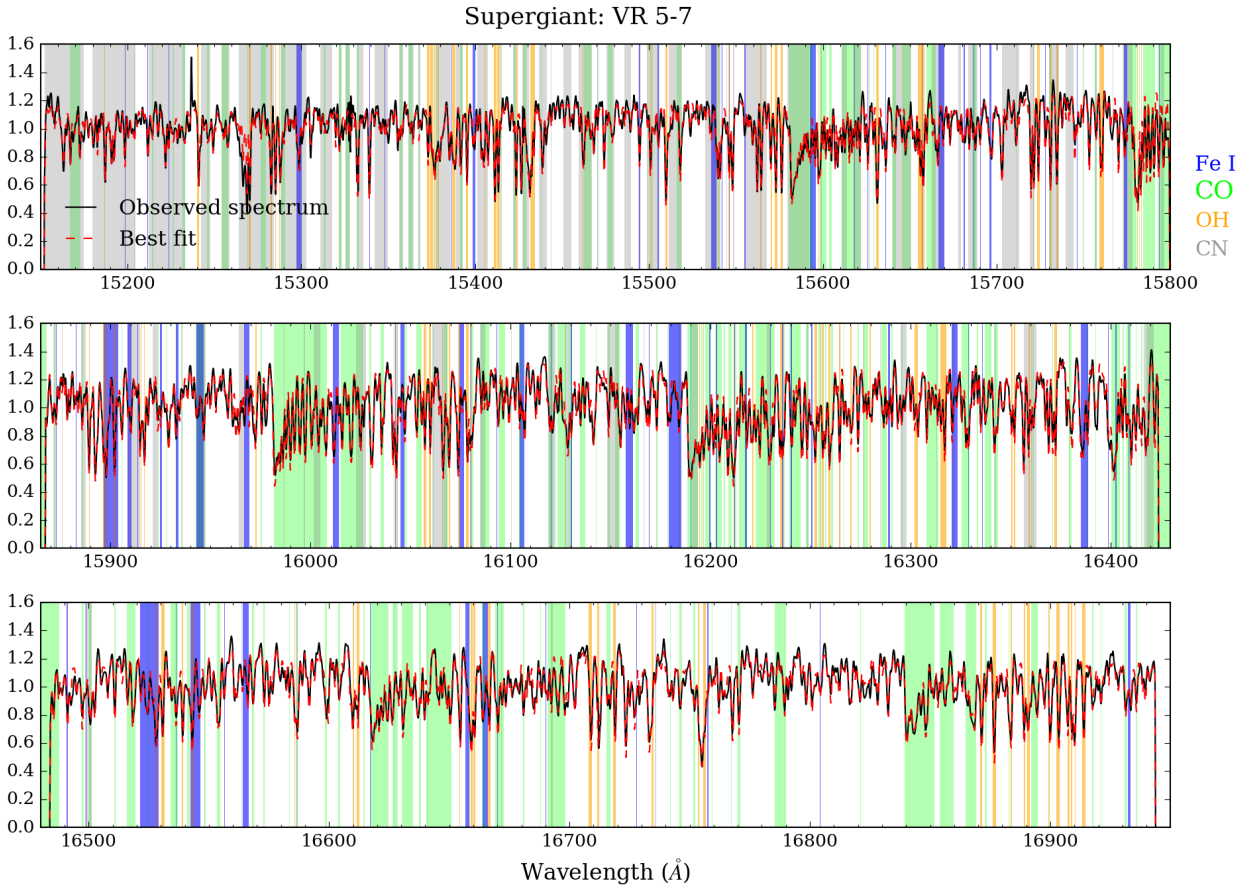

Fig. 4. APOGEE spectrum of supergiant star VR5-7. Black shows the observed spectrum and red the best fit spectrum obtained by the automated APOGEE pipeline ASPCAP. The most prominent molecular bands of CO, CN and OH as well as Fe I lines are also indicated.

cluster), where about 80% of their sample is metal rich. If we apply the same criterion to the GALCEN field, we find about 50% of the stars at $|z| = 0.80$ kpc to be metal rich, in perfect agreement within the inner four degrees as shown in Fig. 4 of Schultheis et al. (2019). This strengthens the evidence for a distinct stellar system in the GC region with respect to the IGB ($|b| < 2°$).

5. Chemical abundances

Schultheis et al. (2015) could only study the general α-element abundances for the GALCEN field with APOGEE DR12, but with DR16 we are able to study the detailed chemistry of the cooler end of the giant branch. We restricted our analysis to regular M giant stars and did not include the known and candidate AGB/supergiants stars. As a comparison sample, we used the Galactic bulge sample by Queiroz et al. (2020b) based on SH distances and the Zasowski et al. (2019) bulge sample, which was updated for DR16. The sample was defined as stars falling inside the galactocentric coordinates $|X| < 5$ kpc, $|Y| < 3.5$ kpc, $|Z| < 1.0$ kpc with an additional cut in the reduced proper motion diagram. We refer the reader to Queiroz et al. (2020b) for a detailed description on their bulge sample. In addition, we restricted our sample to $R_{GC} \leq 3.5$ kpc, leaving about 5800 bulge stars for our comparison shown in Fig. 6. The detailed properties of the comparison bulge sample are discussed in an accompanying paper. Additionally, as a comparison we show the bulge sample of Zasowski et al. (2019), which was updated for DR16.

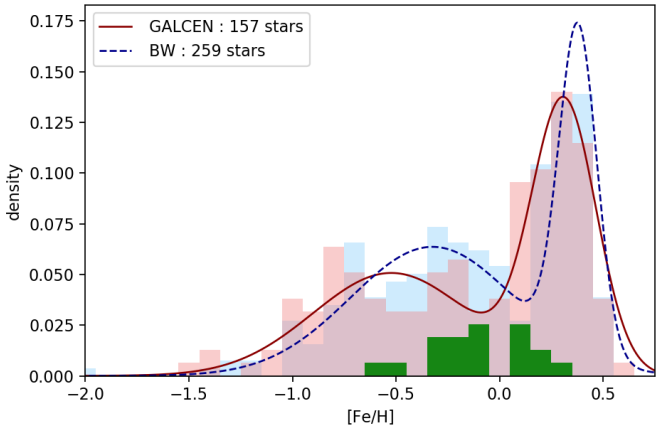

Fig. 5. GMM decomposition of MDF for the GALCEN sample (red) and Baade's window (blue). In green: the known and candidate AGB/supergiant stars (Tables 1 and 2) are indicated. The bin size is 0.1 dex.

We used calibrated chemical abundances and omitted stars for which the individual error on each studied chemical element was larger than 0.02 dex. The overall behaviors for the alpha elements Mg, Si, O, and Ca are shown as a function of [Fe/H] in Fig. 6. Due to the large number of bulge comparison stars, we used densities for the Zasowski et al. (2019) sample and contours for the Queiroz et al. sample (see Fig. 6). In addition, we used samples in the literature of Rich et al. (2012)

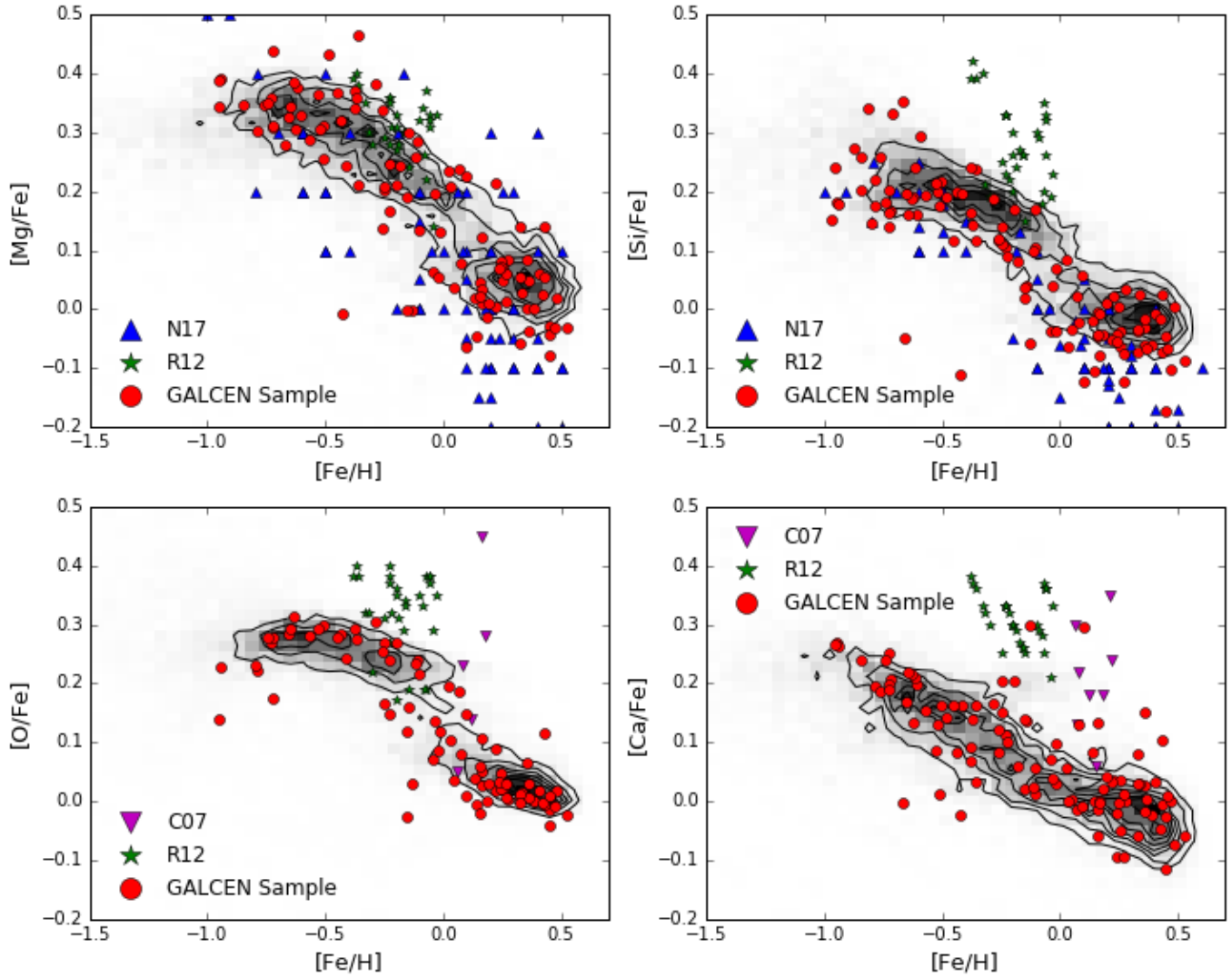

Fig. 6. [Fe/H] vs. [X/Fe] of the alpha-elements, for the APOGEE GALCEN sample. Also shown for comparison are the APOGEE bulge sample of Queiroz et al. (in prep.) as contours, the APOGEE bulge sample of Zasowski et al. (2019, updated for DR16) as shaded density, and literature values for Cunha et al. (2007, C07), Rich et al. (2007, R12), and Nandakumar et al. (2018).

and Nandakumar et al. (2018) for the inner bulge ($|b| < 1°$), and Cunha et al. (2007) for stars in the nuclear star cluster.

The GALCEN stars (black dots) overall follow the same behavior as the Galactic bulge stars of Queiroz et al. (in prep.). Concerning the behavior of APOGEE results for [α/Fe]–[Fe/H] it is clear that Ca shows, compared to the other α-elements, a different behavior where stars with subsolar metallicities are less enhanced compared to Mg, O, and Si; the Ca abundances also decrease for higher metallicities, while the other alpha-elements tend to show a flattening. In the DR16 results, there is a noticeable feature (reminiscent of a "finger:" Jönsson et al. 2020) at [Ca/Fe] $\sim$ +0.25 and [O/Fe] $\sim$ +0.25 and [Fe/H] $>$ 0. Such horizontal sequence of stars had already been noticed for the DR14 results in the inner bulge sample (Zasowski et al. 2019). Jönsson et al. (2020) concluded that the tightness of this feature, which contains about 4% of the main stellar sample of giants, makes it likely that this feature is due to some possible systematics in the abundance determinations, which the APOGEE/ASPCAP team has not yet been able to identify. However, most likely due to our small sample size, we do not find this feature in the GALCEN sample.

As in DR14, we see that the oxygen abundances show the tightest sequence compared to Mg, Si, and Ca, in particular for low metallicities. What is worth mentioning is the extremely flat behavior of oxygen for high metallicities ([Fe/H] $>$ 0.1), as already noted by Zasowski et al. (2019); the DR16 data release using the MARCS models confirms this trend. However, Johnson et al. (2014) found, from their analysis of bulge stars in the optical and by comparing them with values in the literature, that the O-abundances decrease for higher metallicities with no sign of a flattening (see their Fig. 13). So this flattening at higher metallicities found in the APOGEE data has to be taken with caution as it could be an artifact. However, deriving oxygen abundances for high-metallicity stars in the optical can also be challenging. For example, based on high-resolution optical spectra, Santos-Peral et al. (2020) very recently showed that this flattening for the metal-rich stars can be explained by an incorrect continuum normalization. They demonstrate that with a proper continuum normalization, for example the alpha-element Mg decreases steadily with increasing metallicity with no signs of a flattening. From a theoretical point of view, the flattening can be reproduced by increasing the stellar yields for high

metallicities by a factor of 3.5 (see Matteucci et al. 2020) or by radial migration (see e.g., Minchev et al. 2014 and Anders et al. 2017). Si and Mg show very similar trends with a less pronounced knee position than oxygen. Striking for both elements is the flattening at high metallicities, while Nandakumar et al. (2018) show a decreasing trend of Si and Mg for the metal-rich stars. Johnson et al. (2014) show, for their bulge sample, that Mg and Si also decrease with increasing metallicity. Interestingly, the sample of Cunha et al. (2007), which features stars in the nuclear star cluster, are also enhanced, but in a single metallicity.

6. Are the nuclear star disk and the nuclear star cluster chemically distinct?

For their sample of M giants in the NSC, Cunha et al. (2007) already noticed α-enhancement in [O/Fe] and [Ca/Fe] at supersolar metallicities. Recently, Thorsbro et al. (2020) also revealed alpha-enhanced, metal-rich stars in the NSC, which could be sign of a starburst activity initiated by a sudden accretion of gas, be it primordial or slightly enriched. Although their sample is small, and clearly more stars are needed to confirm their results, they show a possible sign of a starburst, making a kind of "loop" structure in the [Si/Fe] vs. [Fe/H] diagram, which can be explained by the following. The sudden accretion of gas will first result in a dilution of chemical abundances (e.g., Fe) before the [Si/Fe] vs. [Fe/H] ratio increases due to the contribution of core-collapse SNe II, followed by a decrease of [α/Fe] due to the Fe production from Type Ia SNe. In our Fig. 6, which probes the NSD, we do not see evidence of alpha-enhanced metal-rich stars, suggesting a chemical distinction between the NSC and the NSD. In addition, Feldmeier-Krause et al. (2020) traced the metallicity distribution function in the NSC based on 600 late-type stars. We compare the MDF in Fig. 7 between their sample and our GALCEN sample, which we restrict to $|b| < 0.4°$ in order to probe the NSD (see Fig. 2). Although only ~50 stars are left over in the NSD, we see that the two MDFs differ, in particular the MDF of the NSD shows a more significant metal-poor tail ([Fe/H] < -0.5) compared to the NSC. Performing a bootstrapping with 1000 resamplings, for the NSD we find the metal-poor peak at -0.57 ± 0.19 dex, while for the NSC is can be found at -0.36 ± 0.12 dex. However, the sample size of the NSD is clearly too small, and more observations are needed.

In addition, we also see differences in their star formation histories. While the majority of stars in the NSC and NSD are old (80% of the stars are ~10 Gyr old), Nogueras-Lara et al. (2019) detected signs of a recent star formation around 1 Gyr ago in the NSC that is not present for the NSC (Pfuhl et al. 2011, Schödel et al. 2020). This strengthens the argument that the NSC and NSD are indeed chemically distinct and these two systems might have formed differently.

7. Kinematics vs. metallicity

We transformed the heliocentric radial velocities to galactocentric velocities according to Schönrich et al. (2015):

$$v_{\rm GC} = v_{\rm rad} + 14 \times \cos(l)\cos(b) + 250 \times \sin(l)\cos(b) + 7 \times \sin(b). \quad (1)$$

Figure 8 shows the normalized galactocentric velocity distribution split in negative and positive longitudes where we confirm the clear signature of the rotation of the nuclear stellar disk as pointed out by Schönrich et al. (2015). However, due to the larger sample size now in GALCEN, we noticed a significant

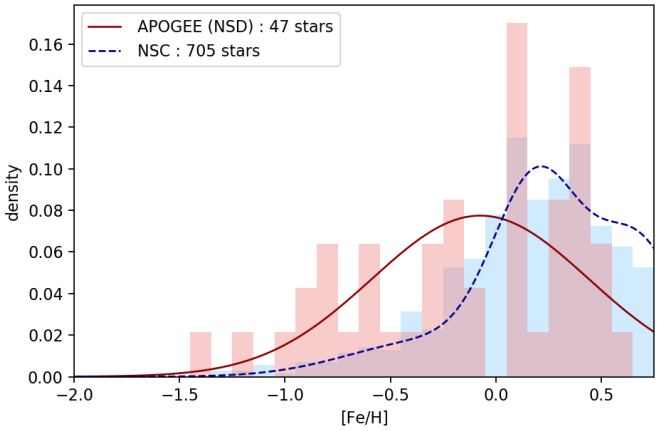

Fig. 7. MDF of the NSC sample of Feldmeier-Krause et al. (2020) compared to the NSD GALCEN sample confined to $|b| < 0.4°$.

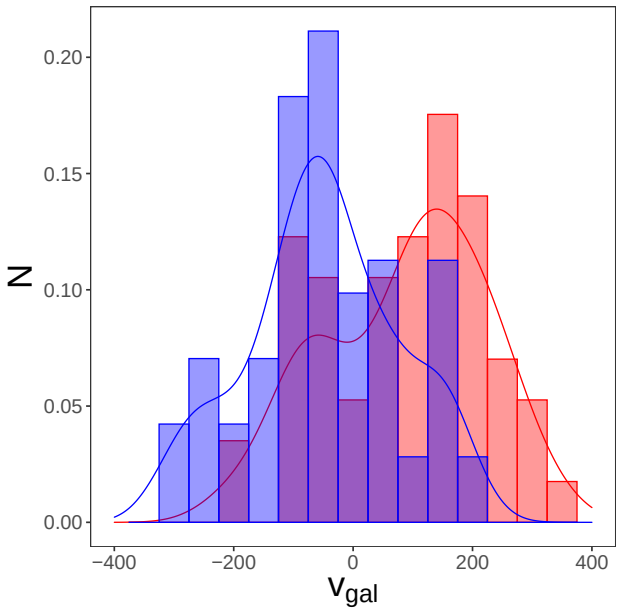

Fig. 8. Normalized galactocentric velocity distributions for negative longitudes and positive longitudes (in red and blue, respectively) as in Schönrich et al. (2015). We limited our sample to $|l| < 0.5°$ in order to account for the uneven sample distribution.

fraction of high velocity stars exceeding 300 km s^{-1}. These high velocity stars have [Fe/H] > -0.5, ruling out any possible connection to the Galactic halo. Do these stars originate from the GC, or could they have been kicked up from a binary supernova explosion, the interaction of a dwarf galaxy or a globular cluster with the disk, or interaction between multiple stars, as proposed by Du et al. (2018)? Proper motion measurements would be necessary to derive the detailed orbits of those stars in order to understand their origin.

The velocity dispersion of the GALCEN sample is 159 km s^{-1}, with a slightly larger dispersion for the metal-rich stars (163 km s^{-1}) with respect to the metal-poor stars (156 km s^{-1}). We define metal rich (MR) and metal poor (MP), as in Zoccali et al. (2017), as [Fe/H] > 0.1 for MR and [Fe/H] < -0.1 for MP. Based on GIBS data, while for higher latitudes the MP population shows a larger velocity dispersion, Zoccali et al. (2017) showed that this trend is inverted by going closer to the plane from $|b| = 1°$ inwards. Based on

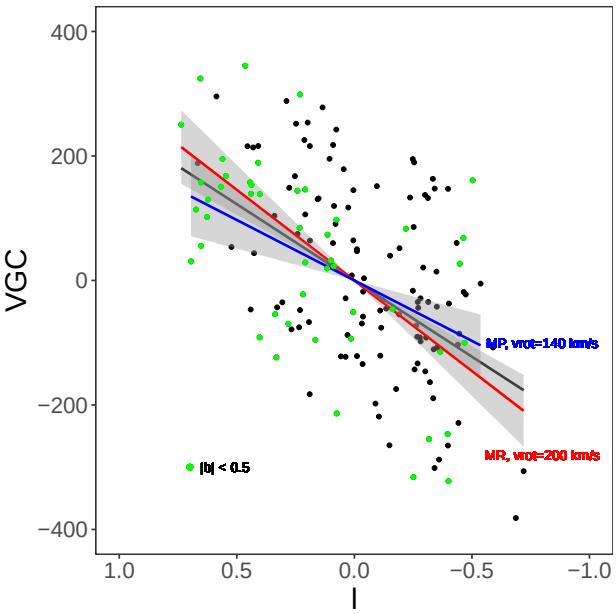

Fig. 9. Galactocentric radial velocity vs. galactic longitude. The black line shows the linear fit of the full GALCEN sample, while the red line shows the fit for metal-rich stars [Fe/H] > 0, and the blue line shows MP stars. The shaded area shows the 95% level of confidence interval. The green points are stars inside 0.4 degrees of galactic latitude. See text for details.

proper motion measurements, Clarkson et al. (2018) found that the metal-rich population shows a steeper rotation curve. Our analysis of GALCEN confirms their results with an increasing velocity dispersion with higher metallicity. Kunder et al. (2016) showed that metal-poor stars such as RR Lyrae rotate much more slowly than RGB or RC stars in the bulge, and they suggested that they belong to the classical bulge. Other studies also reveal the presence of an old population in the GC region (see e.g., Contreras Ramos et al. 2018, Dong et al. 2017, and Minniti et al. 2016). Based on the GIBS RC stars, Zoccali et al. (2017) gave some indications that MP stars show a marginally slower rotation compared to the MR stars (see their Fig. 13). We investigated this in more detail by tracing the slope of the MR and MP stars in the l vs. v_{GC} plane. We used a similar method for the fitting procedure to Schönrich et al. (2015). Figure 9 shows a linear fit of the entire GALCEN sample (black line) as well as the fit for the MR stars (red solid line) and MP stars (blue solid line). The rotational speed can be calculated by assuming a radius for the NSD as shown by Eq. (2), assuming a typical radius R of the NSD of 120 pc:

$$v_{\rm rad} = R_0 \times \sin(l) \times (V/R_{\rm NSD} - V_0/R_0), \quad (2)$$

where $v_{\rm rad}$ is the heliocentric radial velocity, $R_0 = 8.2$ kpc (distance to the GC), $V_0 = 220\,{\rm km\,s^{-1}}$ (sun velocity), l the galactic longitude, and $R_{\rm NSD}$ the radius of the disk (120 pc).

For the best fit (indicated by the blue and red line for both the MP and MR population, respectively), we obtain a rotation velocity of $140 \pm 30\,{\rm km\,s^{-1}}$ for the MP stars and $200 \pm 30\,{\rm km\,s^{-1}}$ for the MR stars, clearly indicating a faster rotation for the MR stars. If we restrict our sample to $|b| \leq 0.4°$, which is the approximate vertical extent of the nuclear stellar disk (see Fig. 2), we obtain very similar fitting results. The reason for this difference in the rotation velocity between MR and MP stars may have a different origin. For example, MP stars could be formed from disrupted stellar clusters. Tsatsi et al. (2017) showed that using N-body simulation of inspiralling clusters to the center of the Milky Way can reproduce both the morphological and kinematical properties of the NSC. On the other hand, Mastrobuono-Battisti et al. (2019) showed that in the presence of an aspherical, time-variable potential (e.g., due to the presence of a discrete stellar black hole cusp), counter-rotating disks can perturb the dynamics of older stellar populations leading to accelerated relaxation, while the younger populations show a larger amount of rotation. Younger populations always show larger rotation compared to older ones, but the difference is even larger for counter-rotating disks. Age information and chemical footprints such as dispersion in light elements (Schiavon et al. 2017) would be essential to understand the different possible formation scenarios.

8. Conclusions

Using the latest DR16 APOGEE data release, we studied cool M giants in the GALCEN sample going down to temperatures of 3200 K. Among those, stellar parameters of a bunch of known and candidate AGB/supergiant stars are now available thanks to the cool grid of MARCS model atmospheres and significant improvements in the analysis of cool stars by the APOGEE/ASPCAP team. The known (6) and candidate (15) AGB/supergiant stars are situated well above the tip of the RGB, confirming their status as cool luminous stars. We confirm that a photometric H–K color cut combined with a dereddened magnitude cut of K_0 is a very powerful criterion to select AGB/supergiant stars. In the MDF of GALCEN, we clearly identify a metal-poor peak at [Fe/H] = −0.53 dex, which is about 0.2 dex lower than the metal-poor peak in BW. About 50% of the stars belong to each of the MR and MP populations. The group of AGB/supergiant stars follows the same trend in the MDF as the normal M giants. The general α-abundances of the GALCEN stars show a very bulge-like behavior. As already pointed out by Schönrich et al. (2015), we identify the rotation of the nuclear disk seen in the galactic longitude vs. v_{GC} diagram. Separating our sample in an MR and MP population, we detect a much higher rotation velocity of the MR stars with $200\,{\rm km\,s^{-1}}$ with respect to the MP stars ($140\,{\rm km\,s^{-1}}$), indicating a different origin of these two populations. We see evidence of clear differences in the chemical footprints of the nuclear disk and the NSCs, both in chemical abundances and the MDF. Together with their different SFH, it is likely that the NSD and the NSC have formed on different time scales.

Acknowledgements. We want to thank the anonymous referee for her/his very fruitful and valuable comments. MS thanks A. Mastrobueno-Battisti for very fruitful discussions. We want to thank Anja Feldmeier-Krause to make their table of metallicities for the NSC available. M. S. acknowledges the Programme National de Cosmologie et Galaxies (PNCG) of CNRS/INSU, France, for financial support. DM is supported by the BASAL Center for Astrophysics and Associated Technologies (CATA) through Grant AFB 170002, by the Programa Iniciativa Científica Milenio grant IC120009, awarded to the Millennium Institute of Astrophysics (MAS), and by Project FONDECYT No. 1170121. DAGH and O. Z. acknowledge support from the State Research Agency (AEI) of the Spanish Ministry of Science, Innovation and Universities (MCIU) and the European Regional Development Fund (FEDER) under grant AYA2017-88254-P. J. G. F.-T. is supported by FONDECYT No. 3180210 and Becas Iberoamérica Investigador 2019, Banco Santander Chile. S. H. is supported by an NSF Astronomy and Astrophysics Postdoctoral Fellowship under award AST-1801940. R. R. M. acknowledges partial support from project BASAL AFB-170002 as well as FONDECYT project N°1170364. Funding for SDSS-III has been provided by the Alfred P. Sloan Foundation, the Participating Institutions, the National Science Foundation, and the US Department of Energy Office of Science. The SDSS-III web site is http://www.sdss3.org/. SDSS-III is managed by the Astrophysical Research Consortium for the

Participating Institutions of the SDSS-III Collaboration including the University of Arizona, the Brazilian Participation Group, Brookhaven National Laboratory, Carnegie Mellon University, University of Florida, the French Participation Group, the German Participation Group, Harvard University, the Instituto de Astrofisica de Canarias, the Michigan State/Notre Dame/JINA Participation Group, Johns Hopkins University, Lawrence Berkeley National Laboratory, Max Planck Institute for Astrophysics, Max Planck Institute for Extraterrestrial Physics, New Mexico State University, New York University, Ohio State University, Pennsylvania State University, University of Portsmouth, Princeton University, the Spanish Participation Group, University of Tokyo, University of Utah, Vanderbilt University, University of Virginia, University of Washington, and Yale University. Funding for the Sloan Digital Sky Survey IV has been provided by the Alfred P. Sloan Foundation, the US Department of Energy Office of Science, and the Participating Institutions. SDSS-IV acknowledges support and resources from the Center for High-Performance Computing at the University of Utah. The SDSS web site is www.sdss.org. SDSS-IV is managed by the Astrophysical Research Consortium for the Participating Institutions of the SDSS Collaboration including the Brazilian Participation Group, the Carnegie Institution for Science, Carnegie Mellon University, the Chilean Participation Group, the French Participation Group, Harvard-Smithsonian Center for Astrophysics, Instituto de Astrofísica de Canarias, The Johns Hopkins University, Kavli Institute for the Physics and Mathematics of the Universe (IPMU)/University of Tokyo, Lawrence Berkeley National Laboratory, Leibniz Institut für Astrophysik Potsdam (AIP), Max-Planck-Institut für Astronomie (MPIA Heidelberg), Max-Planck-Institut für Astrophysik (MPA Garching), Max-Planck-Institut für Extraterrestrische Physik (MPE), National Astronomical Observatories of China, New Mexico State University, New York University, University of Notre Dame, Observatário Nacional/MCTI, The Ohio State University, Pennsylvania State University, Shanghai Astronomical Observatory, United Kingdom Participation Group, Universidad Nacional Autónoma de México, University of Arizona, University of Colorado Boulder, University of Oxford, University of Portsmouth, University of Utah, University of Virginia, University of Washington, University of Wisconsin, Vanderbilt University, and Yale University. We thank the E-Science and Supercomputing Group at Leibniz Institute for Astrophysics Potsdam (AIP) for their support with running the StarHorse code on AIP cluster resources.

References

Ahumada, R., Allende Prieto, C., Almeida, A., et al. 2020, ApJS, 249, 3
Alam, S., Albareti, F. D., Allende Prieto, C., et al. 2015, ApJS, 219, 12
Allende Prieto, C., Beers, T. C., Wilhelm, R., et al. 2006, ApJ, 636, 804
Alvarez, R., & Plez, B. 1998, A&A, 330, 1109
Anders, F., Chiappini, C., Minchev, I., et al. 2017, A&A, 600, A70
Blanton, M. R., Bershady, M. A., Abolfathi, B., et al. 2017, AJ, 154, 28
Carr, J. S., Sellgren, K., & Balachandran, S. C. 2000, ApJ, 530, 307
Clarkson, W. I., Calamida, A., Sahu, K. C., et al. 2018, ApJ, 858, 46
Contreras Ramos, R., Minniti, D., Gran, F., et al. 2018, ApJ, 863, 79
Cunha, K., Sellgren, K., Smith, V. V., et al. 2007, ApJ, 669, 1011
Davies, B., Origlia, L., Kudritzki, R.-P., et al. 2009, ApJ, 694, 46
Dong, H., Schödel, R., Williams, B. F., et al. 2017, MNRAS, 471, 3617
Du, C., Li, H., Liu, S., Donlon, T., & Newberg, H. J. 2018, ApJ, 863, 87
Eisenstein, D. J., Weinberg, D. H., Agol, E., et al. 2011, AJ, 142, 72
Feldmeier-Krause, A., Kerzendorf, W., Do, T., et al. 2020, MNRAS,
Freeman, K., Ness, M., Wylie-de-Boer, E., et al. 2013, MNRAS, 428, 3660
García-Hernández, D. A. 2017, Mem. Soc. Astron. It., 88, 336
García-Hernández, D. A., García-Lario, P., Plez, B., et al. 2006, Science, 314, 1751
García-Hernández, D. A., García-Lario, P., Plez, B., et al. 2007, A&A, 462, 711
García-Hernández, D. A., Manchado, A., Lambert, D. L., et al. 2009, ApJ, 705, L31
García Pérez, A. E., Cunha, K., Shetrone, M., et al. 2013, ApJ, 767, L9
García Pérez, A. E., Allende Prieto, C., Holtzman, J. A., et al. 2016, AJ, 151, 144
Glass, I. S. 1999, in Handbook of Infrared Astronomy, eds. R. Ellis, J. Huchra, S. Kahn, G. Rieke, & P. B. Stetson
Glass, I. S., Matsumoto, S., Carter, B. S., & Sekiguchi, K. 2001, MNRAS, 321, 77
Gonzalez, O. A., Rejkuba, M., Zoccali, M., et al. 2012, A&A, 543, A13
Grieco, V., Matteucci, F., Ryde, N., Schultheis, M., & Uttenthaler, S. 2015, MNRAS, 450, 2094
Gunn, J. E., Siegmund, W. A., Mannery, E. J., et al. 2006, AJ, 131, 2332
Gustafsson, B., Edvardsson, B., Eriksson, K., et al. 2008, A&A, 486, 951
Habing, H. J., & Olofsson, H. 2004, Asymptotic Giant Branch Stars (Springer)
Holtzman, J. A., Shetrone, M., Johnson, J. A., et al. 2015, AJ, 150, 148
Indebetouw, R., Mathis, J. S., Babler, B. L., et al. 2005, ApJ, 619, 931
Johnson, C. I., Rich, R. M., Kobayashi, C., Kunder, A., & Koch, A. 2014, AJ, 148, 67
Jönsson, H., Holtzman, J. A., Prieto, C. A., et al. 2020, AJ, 160, 120
Kunder, A., Rich, R. M., Koch, A., et al. 2016, ApJ, 821, L25
Lançon, A., & Wood, P. R. 2000, A&AS, 146, 217
Launhardt, R., Zylka, R., & Mezger, P. G. 2002, A&A, 384, 112
Liermann, A., Hamann, W. R., & Oskinova, L. M. 2009, A&A, 494, 1137
Majewski, S. R., Schiavon, R. P., Frinchaboy, P. M., et al. 2017, AJ, 154, 94
Mastrobuono-Battisti, A., Perets, H. B., Gualandris, A., Neumayer, N., & Sippel, A. C. 2019, MNRAS, 490, 5820
Matsunaga, N., Kawadu, T., Nishiyama, S., et al. 2009, MNRAS, 399, 1709
Matteucci, F., Vasini, A., Grisoni, V., & Schultheis, M. 2020, MNRAS, 494, 5534
McQuinn, K. B. W., Boyer, M., Skillman, E. D., & Dolphin, A. E. 2019, ApJ, 880, 63
Minchev, I., Chiappini, C., & Martig, M. 2014, A&A, 572, A92
Minniti, D., Contreras Ramos, R., Zoccali, M., et al. 2016, ApJ, 830, L14
Moneti, A., Glass, I. S., & Moorwood, A. F. M. 1994, MNRAS, 268, 194
Nandakumar, G., Ryde, N., Schultheis, M., et al. 2018, MNRAS, 478, 4374
Nidever, D. L., Holtzman, J. A., Allende Prieto, C., et al. 2015, AJ, 150, 173
Nogueras-Lara, F., Schödel, R., Gallego-Calvente, A. T., et al. 2019, Nat. Astron.,
Omont, A., Gilmore, G. F., Alard, C., et al. 2003, A&A, 403, 975
Ortiz, R., Blommaert, J. A. D. L., Copet, E., et al. 2002, A&A, 388, 279
Pastorelli, G., Marigo, P., Girardi, L., et al. 2019, MNRAS, 485, 5666
Pfuhl, O., Fritz, T. K., Zilka, M., et al. 2011, ApJ, 741, 108
Plez, B. 2012, Turbospectrum: Code for Spectral Synthesis (Astrophysics Source Code Library)
Queiroz, A. B. A., Anders, F., Santiago, B. X., et al. 2018, MNRAS, 476, 2556
Queiroz, A. B. A., Anders, F., Chiappini, C., et al. 2020a, A&A, 638, A76
Queiroz, A. B. A , Chiappini, C., Perez-Villegas, A., et al. 2020b, A&A, submitted [arXiv:2007.12915]
Ramírez, S. V., Sellgren, K., Carr, J. S., et al. 2000, ApJ, 537, 205
Rich, R. M., Origlia, L., & Valenti, E. 2007, ApJ, 665, L119
Rich, R. M., Origlia, L., & Valenti, E. 2012, ApJ, 746, 59
Rojas-Arriagada, A., Recio-Blanco, A., Hill, V., et al. 2014, A&A, 569, A103
Ryde, N., & Schultheis, M. 2015, A&A, 573, A14
Santos-Peral, P., Recio-Blanco, A., de Laverny, P., Fernández-Alvar, E., & Ordenovic, C. 2020, A&A, 639, A140
Schiavon, R. P., Johnson, J. A., Frinchaboy, P. M., et al. 2017, MNRAS, 466, 1010
Schödel, R., Nogueras-Lara, F., Gallego-Cano, E., et al. 2020, A&A, 641, A102
Schönrich, R., Aumer, M., & Sale, S. E. 2015, ApJ, 812, L21
Schultheis, M., Lançon, A., Omont, A., Schuller, F., & Ojha, D. K. 2003, A&A, 405, 531
Schultheis, M., Chen, B. Q., Jiang, B. W., et al. 2014, A&A, 566, A120
Schultheis, M., Cunha, K., Zasowski, G., et al. 2015, A&A, 584, A45
Schultheis, M., Rojas-Arriagada, A., García Pérez, A. E., et al. 2017, A&A, 600, A14
Schultheis, M., Rich, R. M., Origlia, L., et al. 2019, A&A, 627, A152
Thorsbro, B., Ryde, N., Rich, R. M., et al. 2020, ApJ, 894, 26
Tsatsi, A., Mastrobuono-Battisti, A., van de Ven, G., et al. 2017, MNRAS, 464, 3720
Wilson, J. C., Hearty, F. R., Skrutskie, M. F., et al. 2019, PASP, 131, 055001
Wood, P. R., Habing, H. J., & McGregor, P. J. 1998, A&A, 336, 925
Zamora, O., García-Hernández, D. A., Allende Prieto, C., et al. 2015, AJ, 149, 181
Zasowski, G., Johnson, J. A., Frinchaboy, P. M., et al. 2013, AJ, 146, 81
Zasowski, G., Cohen, R. E., Chojnowski, S. D., et al. 2017, AJ, 154, 198
Zasowski, G., Schultheis, M., Hasselquist, S., et al. 2019, ApJ, 870, 138
Zoccali, M., Vasquez, S., Gonzalez, O. A., et al. 2017, A&A, 599, A12

Appendix A: List of APOGEEIDs

Table A.1. APOGEEIDs used in this paper for the analysis.

APOGEEID		
2M17411696-2845379	2M17444724-2834457	2M17475364-2916499
2M17415562-2854231	2M17445535-2822120	2M17475394-2933090
2M17420041-2851435	2M17445978-2804160	2M17475847-2938176
2M17420630-2846179	2M17450076-2831319	2M17480068-2939462
2M17422063-2852202	2M17450464-2819092	2M17480297-2943223
2M17422591-2901282	2M17450767-2840324	2M17480327-2923540
2M17423476-2851278	2M17452445-2810402	2M17480578-2918285
2M17423502-2849086	2M17452504-2808295	2M17480583-2925217
2M17423812-2850540	2M17453070-2815270	2M17480772-2913302
2M17423924-2840140	2M17453887-2833047	2M17480997-2924080
2M17425347-2853162	2M17454263-2811016	2M17481444-2924176
2M17430180-2837301	2M17454276-2805089	2M17481500-2923220
2M17430420-2908362	2M17454586-2826088	2M17481744-2846454
2M17430697-2904104	2M17455438-2819028	2M17481945-2828585
2M17430939-2911452	2M17460129-2821004	2M17481975-2941196
2M17431183-2805302	2M17460483-2948059	2M17482095-2931181
2M17431215-2836211	2M17461894-2952180	2M17482165-2849161
2M17431579-2837552	2M17462218-2831155	2M17482614-2903377
2M17431676-2854588	2M17462609-2934081	2M17482665-2921284
2M17432025-2835065	2M17462725-2935241	2M17482684-2939452
2M17433138-2835128	2M17463316-2925543	2M17483299-2920129
2M17433323-2825538	2M17463977-2915532	2M17483375-2936066
2M17433389-2832086	2M17464346-2946229	2M17483681-2919095
2M17433811-2833452	2M17465147-2936351	2M17483704-2926399
2M17433895-2839578	2M17465235-2928073	2M17483843-2900451
2M17433960-2803317	2M17470230-2945086	2M17483965-2907047
2M17433967-2908204	2M17470331-2931348	2M17484023-2851445
2M17434212-2810387	2M17470591-2925483	2M17484069-2836340
2M17434430-2840387	2M17470766-2933217	2M17484277-2928243
2M17434549-2819343	2M17471090-2927321	2M17484716-2902130
2M17434740-2821036	2M17471201-2932176	2M17484806-2849357
2M17434955-2835372	2M17471507-2928550	2M17484808-2919367
2M17435231-2836460	2M17471743-2903217	2M17484937-2922212
2M17435923-2828184	2M17471767-2927285	2M17485023-2857537
2M17440216-2830017	2M17471773-2934473	2M17485464-2932428
2M17440516-2825596	2M17471958-2901456	2M17485511-2908256
2M17440701-2830436	2M17472118-2943123	2M17485976-2837160
2M17441037-2827035	2M17472195-2932073	2M17490081-2906543
2M17441210-2825556	2M17472783-2941543	2M17490234-2917537
2M17441310-2829287	2M17473007-2939215	2M17490306-2912438
2M17441358-2803383	2M17473184-2931553	2M17490612-2926138
2M17441648-2844195	2M17473220-2942431	2M17490863-2922031
2M17442423-2841005	2M17473329-2929159	2M17491129-2918514
2M17442477-2830118	2M17473512-2944254	2M17491775-2902183
2M17442705-2832044	2M17473827-2825007	2M17492165-2919289
2M17442986-2838590	2M17473854-2931466	2M17492184-2909233
2M17443100-2823357	2M17474071-2936281	2M17492271-2922456
2M17443315-2830321	2M17474101-2925572	2M17492669-2909339
2M17444047-2903581	2M17474135-2933431	2M17493231-2917440
2M17444090-2914204	2M17474542-2934350	2M17493249-2916168
2M17444213-2820294	2M17474997-2924254	2M17493309-2857103
2M17444222-2841485	2M17475052-2926175	
2M17444388-2832377	2M17475074-2931190	

Notes. The preliminary reduction version r13 has been used with the corresponding allStar-r13-l33-58672.fits file. This file will be provided once the official data release DR17 becomes public.